

UC Berkeley

UC Berkeley Previously Published Works

Title

Slags as Evidence for Copper Mining above Casaccia, Val Bregaglia (Central Alps)

Permalink

<https://escholarship.org/uc/item/54d0b2nq>

Journal

Minerals, 9(5)

ISSN

2075-163X

Authors

Wenk, Hans-Rudolf
Yu, Rong
Tamura, Nobumichi
[et al.](#)

Publication Date

2019



DOI

10.3390/min9050292

Peer reviewed

Article

Slags as Evidence for Copper Mining above Casaccia, Val Bregaglia (Central Alps)

Hans-Rudolf Wenk ^{1,*} , Rong Yu ^{1,2}, Nobumichi Tamura ³ , Duri Bischoff ⁴ and Walter Hunkeler ⁵

¹ Department of Earth and Planetary Science, University of California, Berkeley, CA 94720, USA

² School of Urban Planning and Municipal Engineering, Xi'an Polytechnic University, Xi'an 710048, China; yurong365@vip.163.com

³ Advanced Light Source, Lawrence Berkeley Laboratory, Berkeley, CA 94720, USA; ntamura@lbl.gov

⁴ Independent Researcher, 7602 Casaccia GR, Switzerland; dlb@gm.ch

⁵ Independent Researcher, 7610 Soglio GR, Switzerland; husoglio@bluewin.ch

* Correspondence: wenk@berkeley.edu

Received: 4 March 2019; Accepted: 8 May 2019; Published: 12 May 2019



Abstract: Slags from the remote Mota Farun locality above Casaccia (Val Bregaglia, Swiss Alps) have been analyzed with scanning electron microscopy, X-ray powder diffraction and microfocus synchrotron X-ray diffraction to determine mineralogical composition and microstructures. Non-magnetic slag samples are largely composed of euhedral and dendritic iron-rich olivine in a glassy matrix. Locally there are zones with globular inclusions rich in bornite ((Cu₅Fe)S₄) and locally metallic copper. Some regions display dendritic pentlandite ((Fe,Ni)₉S₈). Magnetic samples are mainly composed of fayalite (Fe₂SiO₄) and wüstite (FeO), with minor magnetite (Fe₃O₄). The mineralogical composition indicates that slags were the product of copper smelting. The slag compositions and morphologies are analogous to slags described from the Oberhalbstein (Graubünden, Switzerland) and the Trentino Alps (Italy) which are attributed to metallurgical exploitations of the Late Bronze Age. While the origin of the ore could not be determined, it may be related to ore deposits of chalcopyrite in greenschists and serpentinites in the vicinity, such as Alp Tgavretga (Septimer Pass) and Val Perossa (Val Bregaglia).

Keywords: copper smelting; slags; Swiss alps; Casaccia; scanning electron microscopy; synchrotron X-rays

1. Introduction

Ancient metallurgy in Europe has been of longstanding interest [1–11] and particularly prehistoric copper production in the eastern Alps received a lot of attention such as the the Oberhalbstein in Graubünden (Switzerland) [12], Montafon [13,14], the Silvretta region [15], Kitzbühel [16], Mitterberg [16,17] and Obersteiermark [18] in Austria and the Trentino region in northern Italy [19–22]. Similar Bronze Age activities have been described from the Western Alps [23]. Copper smelting slags are often found at remote places, corresponding to local mineral deposits, mainly of chalcopyrite.

In 1972 Remo Maurizio [24] described slags from a locality above Casaccia, Val Bregaglia, in the Swiss southern Alps. These slags were never analyzed in any detail and attracted our interest in connection with geological fieldwork [25].

The Casaccia locality is not very far from other mining sites further north in Graubünden where metal mining and processing started in the Bronze age [26], continued through the Middle Ages to the late 19th century [27–30]. Compared with other metallurgical mining operations in the Alps described in the literature [11], Casaccia slags originate from a very small and local operation.

Casaccia is in uppermost Val Bregaglia, which has been an important trading route for a long time. While there is currently no evidence for prehistoric habitation, Romans traversed the Alps from Italy through what is now Casaccia, both over Septimer Pass and over Maloja-Julier Passes, with some relics preserved such as pillars on Julier Pass as well as remains of roadways.

Figure 1 shows a map of upper Val Bregaglia with principal tectonic units compiled from previous studies [25,31,32]. The geology is rather complex, with lower Pennine nappes on the southwest overlain by Austroalpine nappes on the northeast. The Pennine nappes (Suretta, Lizun, Avers and Platta) are composed largely of muscovite-chlorite gneiss, some marble and with local serpentinite. They represent a Paleozoic-Mesozoic basement that was metamorphosed during the early Tertiary Alpine orogeny. The Austroalpine Margna and Err nappes represent largely Hercynian granite, also subjected to Alpine metamorphism and deformation. On the lower right corner of the map is the young Tertiary Bergell granite surrounded by the Forno contact zone. During the ice age, lasting until about 10,000 years BP, much of the area and particularly the valleys were covered by large glaciers, most importantly a glacier from Val Forno (southeast) that divided at Maloja into a branch that moved northeast into the Engadine, and a branch that moved southwest into Val Bregaglia and towards the current Lake of Como. Around 1500 BC and 0 AD there were warm periods, probably with minimal glaciation.

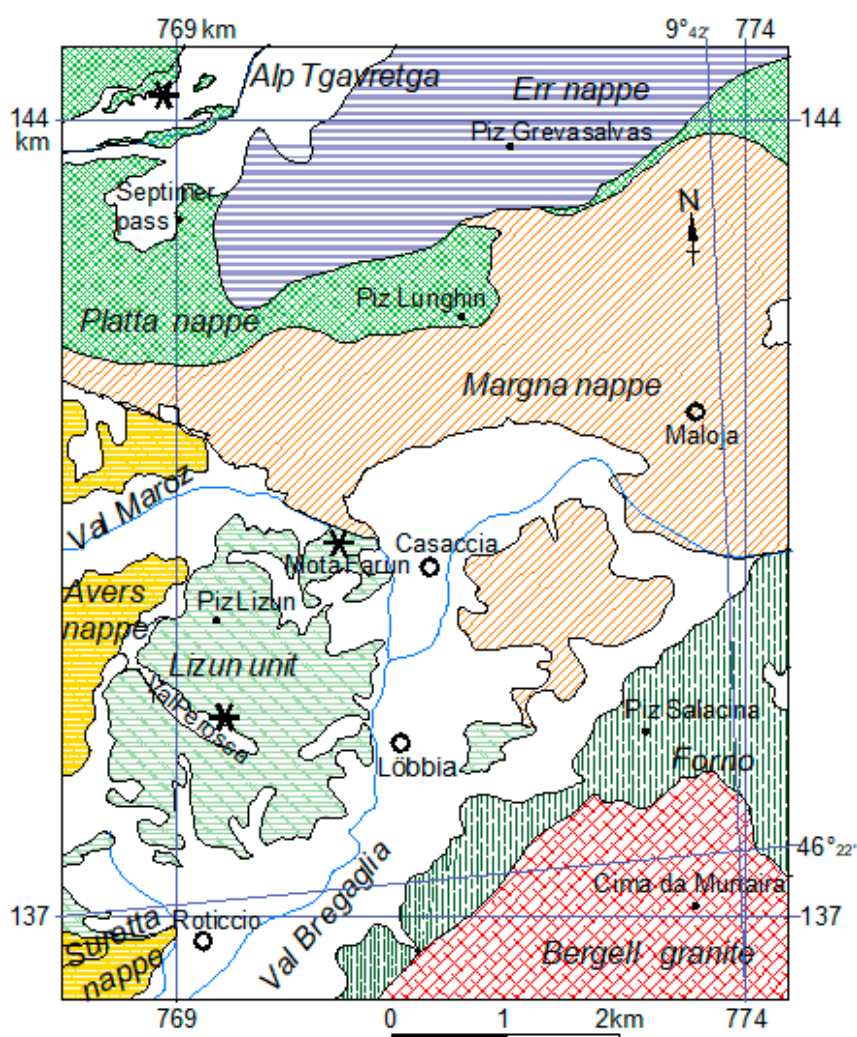


Figure 1. Map of upper Val Bregaglia in the Swiss Alps with tectonic units (italic). The slag locality of Mota Farun and the ore deposits at Alp Tavretga and Val Perossa are indicated by asterisk symbols. Coordinates with a square kilometer scheme are from Swiss topographic maps. Universal geographic coordinates (NS and EW) are also indicated.

Here we study samples of slag from the Casaccia site [24] in some detail with modern methods used in mineralogy to characterize microstructures, identify phases and their morphology. Apart from analyzing slags we also explore potential source material in the vicinity. This may inspire more systematic archeological studies of the Casaccia samples, to identify remains of smelting facilities, radiocarbon age determinations and locating the origin of the ore that was processed in Val Bregaglia. It also could encourage archeologists to apply these methods to explore details of microstructural features to slags from classical sites of ancient metal production. They have mainly relied on conventional geochemistry.

2. Sample Description and Analytical Methods

The map in Figure 1 shows the locality Mota Farun west of Casaccia where Maurizio collected slags [24]. This place is on a steep slope, 200 m above Casaccia (Swiss coordinates 140.3 km/770.6 km, 1600 m), now covered largely by Quaternary debris and forests. Here we collected new samples. The location is in the Pennine Lizun nappe of greenschist metamorphic grade with dominant muscovite-chlorite-albite gneiss.

Slags at the Mota Farun locality occur in various sizes, the largest about 20 cm. They have mainly been found in places of recent erosion (e.g., in connection with lumbering) or excavations (for an adjacent electric power line). No evidence for mining activities could be identified nor could relics of smelters be found. Figure 2 is an image of various slags. Some are homogeneous, others have inclusions of host rock (Figure 2c). Some slags, particularly those with platelet morphology, are strongly magnetic (Figure 2a,b). Most do not display significant magnetism.

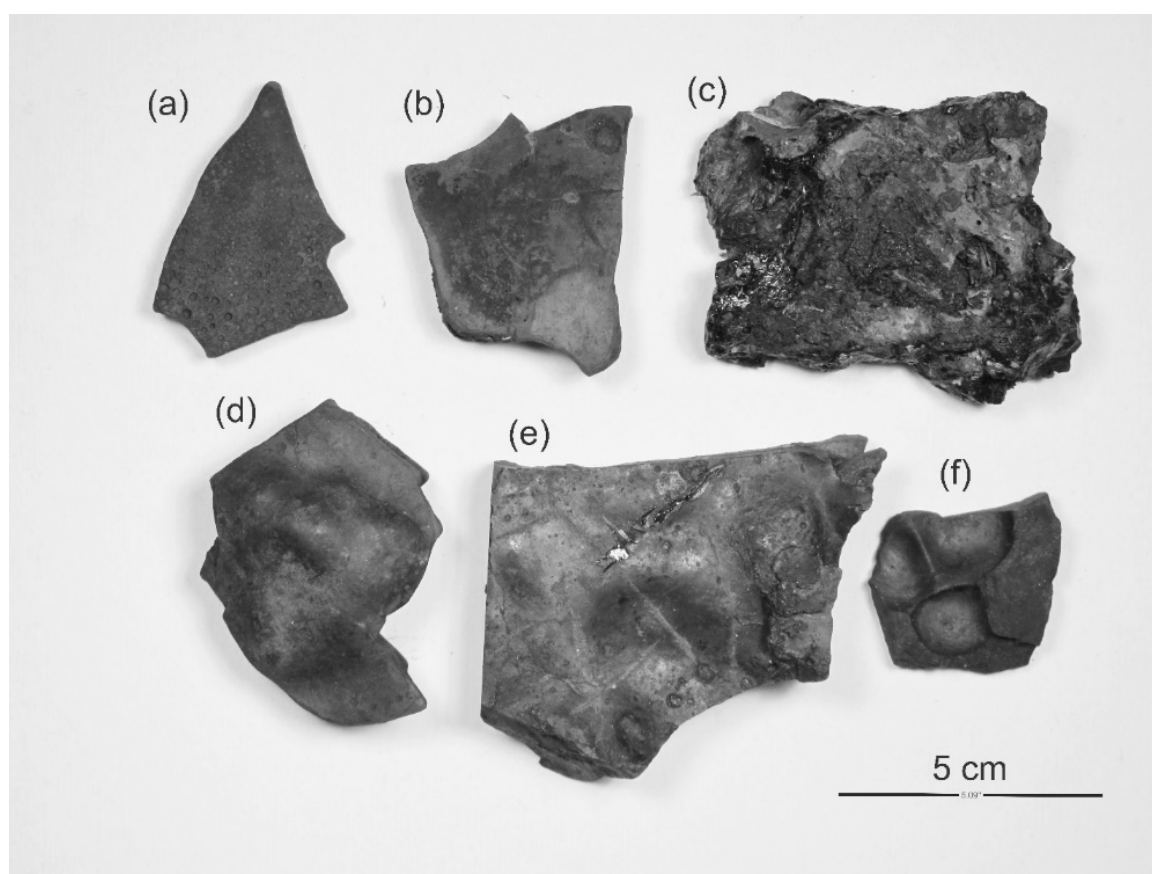


Figure 2. Photograph of Casaccia slags. (a,b) Plate-shaped magnetic slags; (c) slag with inclusions of host rock and (d–f) non-magnetic slags with bulges.

From samples chosen for this study polished 30 μm thin sections were prepared and viewed with optical microscopy to identify areas of interest. These were then analyzed with a Zeiss-Evo scanning electron microscope (SEM) at UC Berkeley. The SEM was operated at 20 kV. For imaging backscatter electrons (BSE) were used to highlight variations in atomic weight. Samples were studied both at low vacuum (requiring no carbon coating) and at high vacuum (with carbon coating). High vacuum microscopy provides higher resolution for BSE images. The chemical composition was assessed with energy-dispersive spectroscopy in the SEM, using an EDAX detector and data processing software. At low vacuum and without carbon coating, low atomic number elements such as carbon and oxygen can be detected. Due to the small grain size of many crystallites, and corresponding averaging in the electron beam, volume fractions of elements are qualitative estimates, particularly for oxygen.

In addition the bulk mineralogical composition of the slags was determined with X-ray powder diffraction (XRD), using an X'Pert Malvern Panalytical system with monochromatic $\text{Co K}\alpha$ radiation (wavelength 1.7902 Å). The X-ray diffraction patterns were analyzed with the Rietveld software MAUD [33].

Two samples were also investigated with synchrotron X-ray micro-diffraction at beamline 12.3.2 of the advanced light source, Lawrence Berkeley National Laboratory, to identify local phases by X-ray diffraction at the micron scale. The instrument used a $5 \times 2 \mu\text{m}^2$ monochromatic beam of 1.23986 Å wavelength. X-ray diffraction images were collected in transmission geometry with a DECTRIS Pilatus 1M area detector (DECTRIS, Baden, Switzerland) positioned at a $\sim 40^\circ$ angle with respect to the incident X-ray beam and at a distance of approximately 185 mm from the sample. For these experiments thin sections of the samples were removed from glass slides and mounted on an aluminum frame. The 2D diffraction images were then analyzed using the XMAS software [34] to identify phases present in local regions.

3. Results

XRD on powders provided some information about the bulk mineralogical composition with olivine (volume fraction $\sim 95\%$, Ol), pyrrhotite ($\sim 4\%$, Po) and some magnetite ($<1\%$, Mag) for non-magnetic slags (Figure 3a), and fayalite ($\sim 55\%$, Fa), wüstite ($\sim 42\%$, Wus) and magnetite ($\sim 3\%$, Mag) for magnetic slags (Figure 3b). Volume fractions of phases were obtained from the MAUD Rietveld refinement [34]. Dots in the spectra represent measured intensities and the line is the corresponding Rietveld fit. For some peaks diffraction indices are shown. The relatively high background between 25° and 50° 2θ in Figure 3a was probably due to an amorphous phase.

SEM-BSE images display complex microstructures. In one sample (Figure 2d) olivine crystals of various morphologies in an amorphous matrix dominate (Figure 4a). Some regions were enriched in metallic globules (bright areas in Figure 4b). Figure 4c–f display a region with a metallic nodule at higher magnification. Figure 4c,e, at higher brightness, emphasized olivine microstructures ranging from euhedral to acicular and dendritic. Particularly Figure 4e illustrates large olivine crystals with zoning, expressed by changes in brightness. The outermost zone was brightest, indicative of high iron content. Figure 4d,f is at low brightness to illustrate microstructures in metallic nodules, divided into regions with brighter and darker grey shades.

To get more information about mineral compositions elemental maps were recorded with energy dispersive spectroscopy (EDS, Figure 5). Results for a region indicated by a square in Figure 4b display olivine with variable Fe and Mg content (Mg, Si, Fe) in an amorphous matrix composed of Al, Mg, Si and Ca. The metal-rich area was composed of Fe-sulfide (darker in Figure 4f and identified as pyrrhotite Po) and Cu-Fe-sulfide (brighter in Figure 4f, identified as bornite Bn). There were some bright spots in Figure 4f attributed to native copper (Cu), as well as in EDS scans (Figure 5), and also of Fe-Ni-sulfide (pentlandite, Pn).

Figure 6 highlights another complex region of a non-magnetic slag (sample in Figure 2e). To display the microstructure with zoned prismatic olivines and olivine dendrites in a darker matrix, relatively high brightness has to be used which makes it difficult to display complexities of sulfide and metallic

phases (Figure 6a). This sample has a higher proportion of metal sulfides in nodules (bornite, Bn and pyrrhotite Po) and metallic copper, which are best visible at lower brightness (Figure 6b). Compositional variations are again displayed in EDS maps (Figure 7) which highlight a matrix high in Al and Ca, as well as a higher concentration of Si than olivine. It also shows a zone of elemental copper (Cu in Figure 6b).

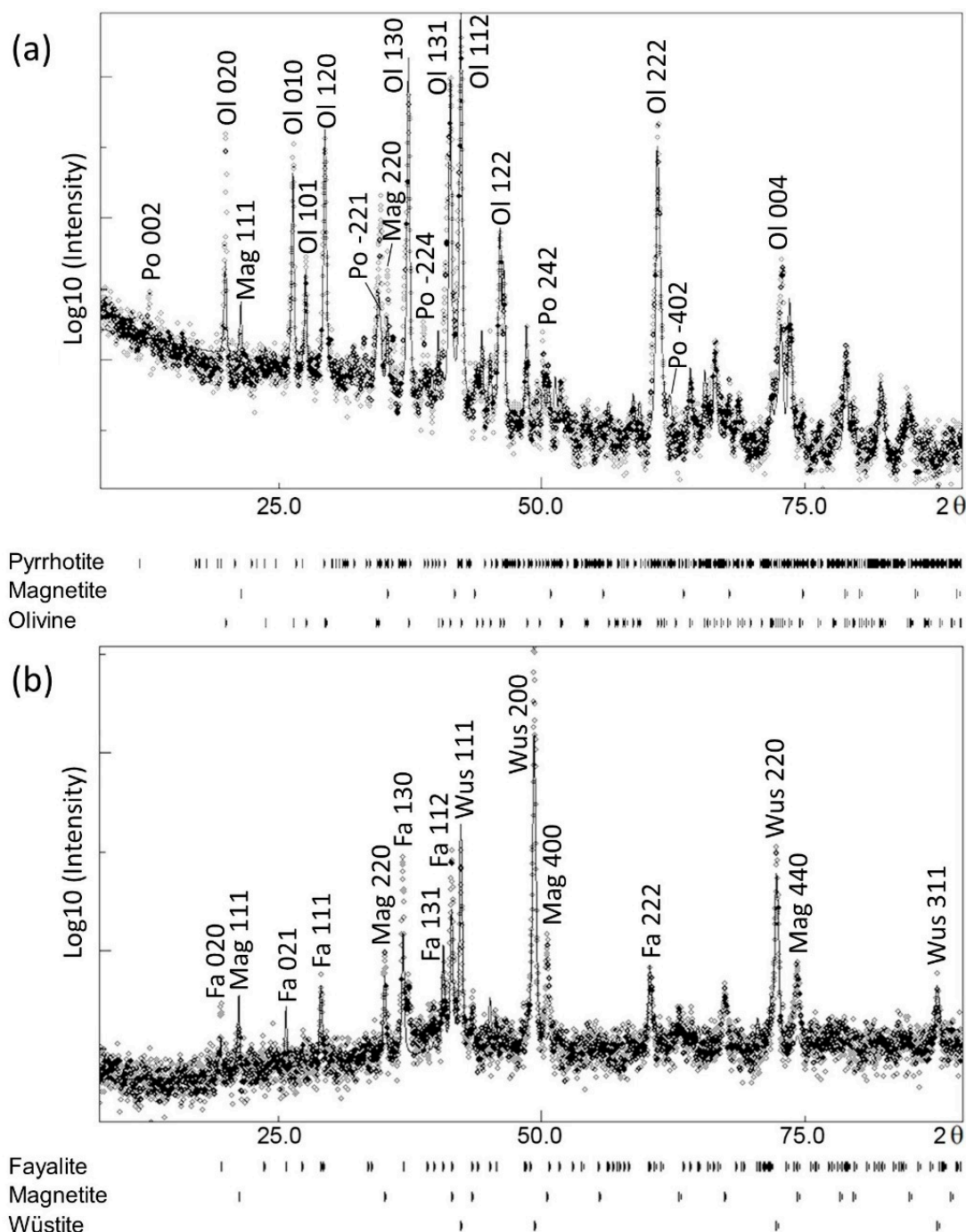


Figure 3. XRD patterns of Casaccia slags plotting intensity (logarithmic scale) as function of 2θ; Co-Kα-radiation. (a) Non-magnetic; (b) magnetic. Dots are measured data and line is Rietveld fit. Some peaks are identified. Phase abbreviations refer to the IUGS convention [35].

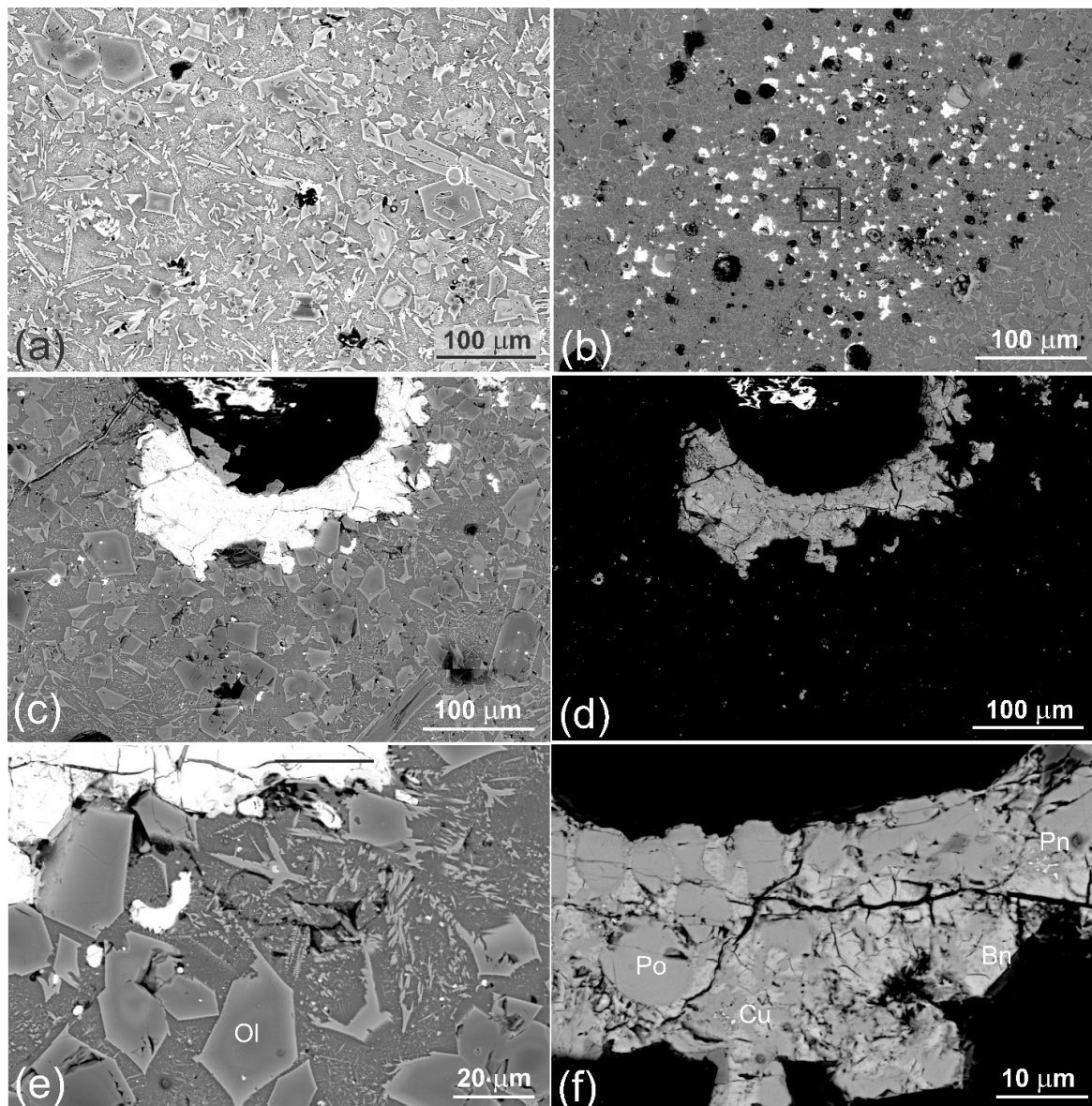


Figure 4. SEM-backscatter electron (SEM-BSE) images of a sample of non-magnetic slag (Figure 2d). (a) Zoned prismatic olivine (Ol) crystals, Fe-rich at the rim, in a matrix with skeletal olivine and olivine dendrites. (b) Region with a concentration of Cu-Fe rich sulfide nodules. The rectangle in the center is the area on which a SEM-energy dispersive spectroscopy (SEM-EDS) scan was performed (Figure 5). (c,d) Region rich in Cu-Fe sulfides (top) in a matrix of olivine (bottom). (c) High brightness to emphasize the olivine matrix, (d) Low brightness to emphasize sulfides. (e) Enlarged area of (c) illustrating euhedral zoned olivine and skeletal olivine in the matrix. (f) Enlarged area of (d) with pyrrhotite (Po), bornite (Bn), copper (Cu, white dots) and pentlandite (Pn, white dots). Abbreviations for minerals here and in other figures refer to IUGS convention [35].

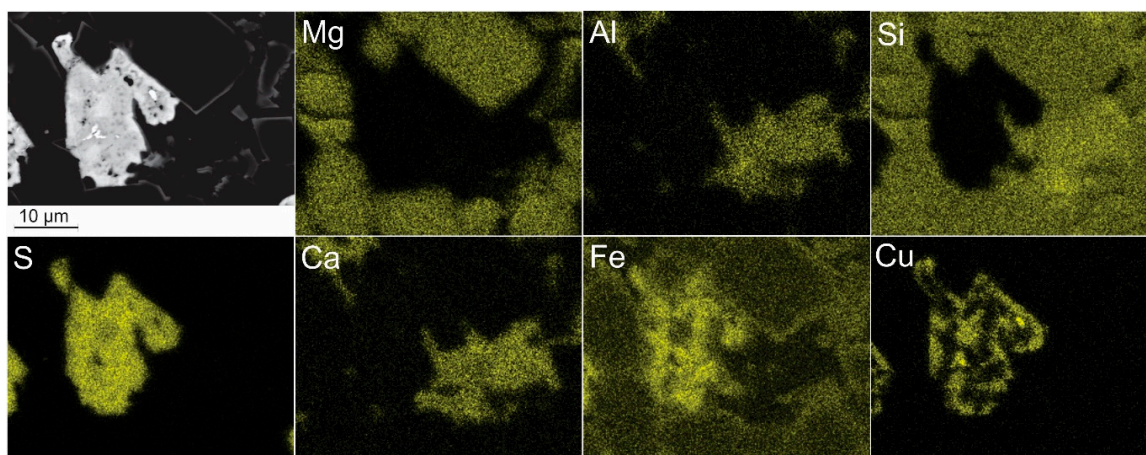


Figure 5. SEM-EDS maps displaying the elemental abundance in a small area highlighted in Figure 4b. First image is SEM-BSE. Areas rich in Al, Ca and Si correspond to the amorphous matrix. High brightness in Cu is elemental copper.

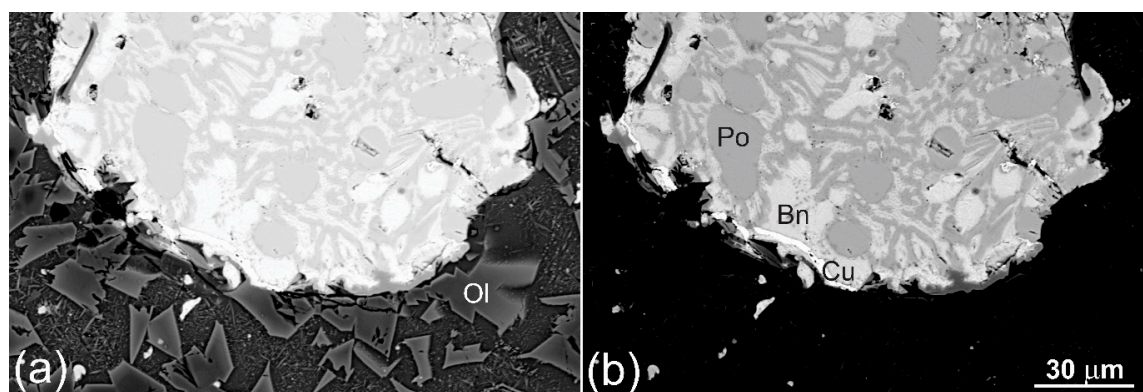


Figure 6. SEM-BSE images of a sample of non-magnetic slag (Figure 2e). Cu-Fe sulfide nodule (bright) composed of pyrrhotite (Po), bornite (Bn) and elemental copper (Cu, white line) in a matrix of zoned prismatic olivine (Ol) crystals. Both images are of the same area and the same magnification (scale in (b) applies to both figures) but (a) is at high brightness to emphasize olivine microstructure and (b) at lower brightness to display complex intergrowth structures of sulfides.

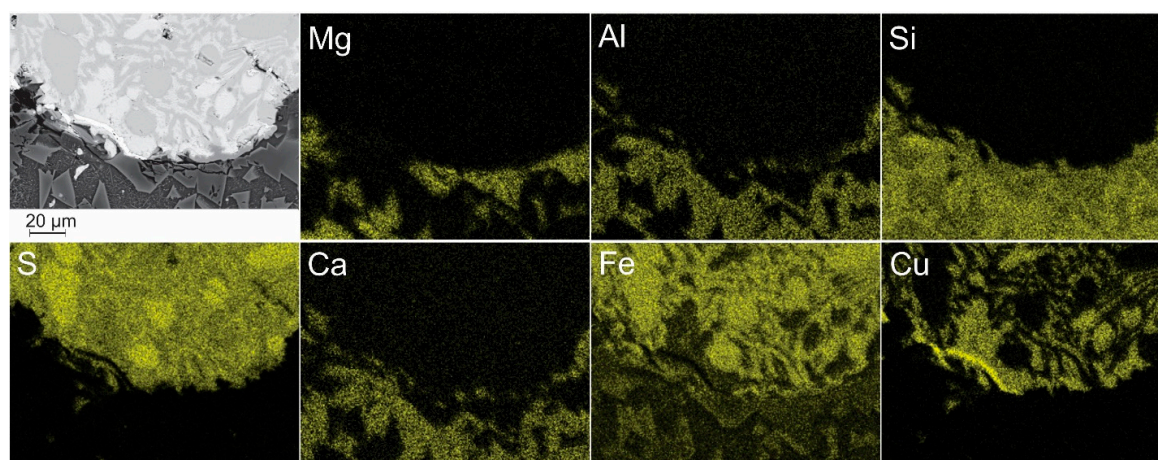


Figure 7. SEM-EDS maps displaying the elemental abundance in the area displayed in Figure 6. First image is SEM-BSE. Areas rich in Al, Ca and Si correspond to the amorphous matrix. High brightness in Cu map is elemental copper and medium brightness is bornite.

A third sample (Figure 2f) was analyzed in some detail (Figure 8). Again SEM-BSE images illustrated a microstructure with euhedral prismatic crystals of olivine with zoning expressed by changes in brightness (Figure 8a). The iron content was highest at the surface and intermediate at the core. An EDS spectrum for the core is shown in Figure 9a. The olivine composition of the core was about $(Mg_{0.75}Fe_{0.25})SiO_4$, at the surface it was $(Mg_{0.5}Fe_{0.5})SiO_4$. The dark glassy matrix, which accounted for about 20% of the volume, was composed of Fe-Al-Mg-Ca-Si-O (Figure 9b), with dendrites of olivine rich in Fe (Figure 8a). Regions of metal-rich nodules occurred in clusters (Figure 8b,c). The bulk is of bornite composition $(Cu_{3.5}Fe_{1.5})S_4$ (Figure 9c) with regions of Fe-S corresponding to pyrrhotite FeS (Figure 9d). Locally there was elemental copper (Figure 8c,d and Figure 9e). Also, again in some areas FeNiS were documented (Figure 9f) with dendritic morphology (Figure 8d). The composition suggests pentlandite $(Fe,Ni)_9S_8$.

While the three non-magnetic slags, which were analyzed (Figure 2d–f), had similar microstructures (Figures 4, 6 and 8), the platy magnetic slags (Figure 2a,b) were entirely different. Figure 10 (corresponding to Figure 2a) displays grey skeletal crystals in a matrix of dark prismatic crystals and occasional bright globules. At higher magnification (Figure 10b) it becomes obvious that the grey crystals were composed of two different phases (brighter and darker grey shades) and also the bright globules were not homogeneous.

With EDS maps (Figure 11) the dark prismatic crystals could be identified as fayalite (Fe_2SiO_4) , grey skeletal crystals as iron oxides wüstite (FeO) and magnetite (Fe_3O_4) and the bright globules as copper-iron-sulfide (bornite). The very dark matrix (Figure 10a) was dominantly composed of Al, Si and Ca (Figure 11).

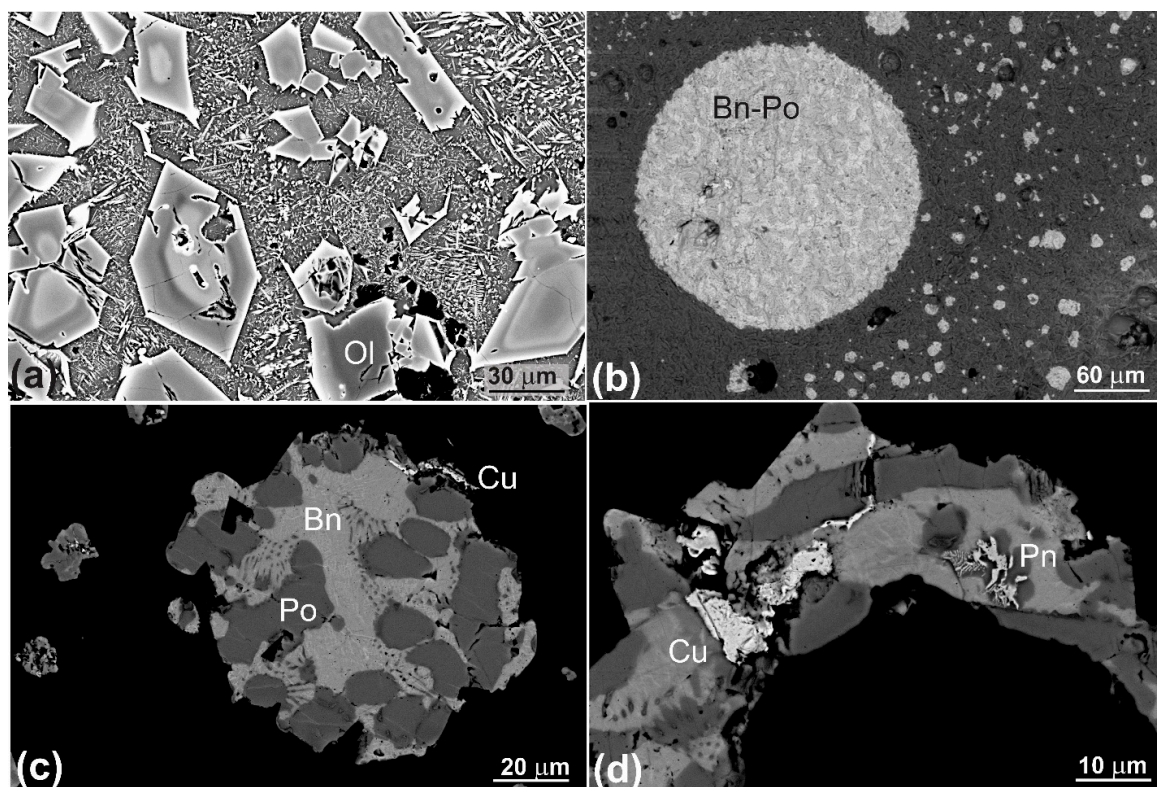


Figure 8. SEM-BSE images of a non-magnetic slag (Figure 2f). (a) Zoned prismatic olivine (Ol) crystals, Fe-rich at the rim, in a matrix with olivine dendrites. (b) Spherical nodule with bornite (Bn, bright) and pyrrhotite (Po, grey). (c) Metallic nodules with pyrrhotite (dark), bornite (grey) and metallic copper (Cu, white). (d) Bornite-pyrrhotite nodule with metallic copper (white on left side) and dendritic pentlandite (Pn, FeNiS) on right side.

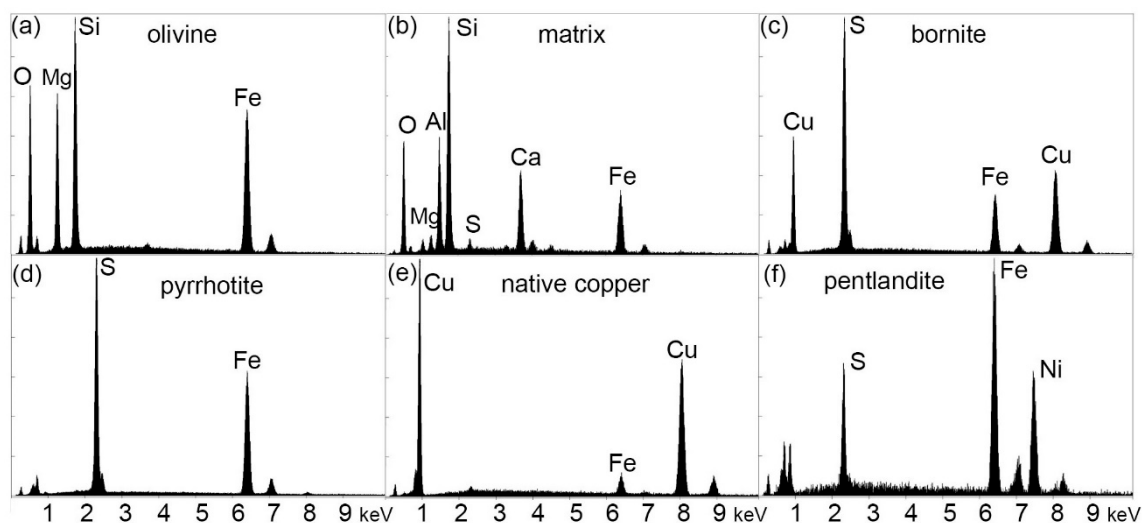


Figure 9. Selected SEM-EDS spectra illustrating composition of non-magnetic Casaccia slag; (a) olivine core (from Figure 8a); (b) amorphous matrix (from Figure 8a); (c) bornite (from Figure 8c); (d) pyrrhotite (from Figure 8c); (e) native copper (from Figure 8d); (f) pentlandite (from Figure 8d). Only K α and L α peaks are labeled; vertical axis is count intensity.

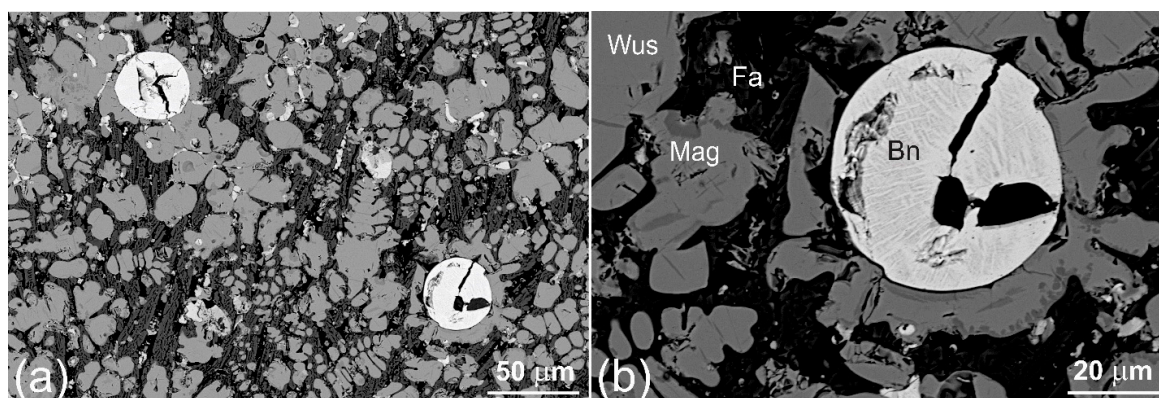


Figure 10. SEM-BSE images of a sample of magnetic slag (Figure 2a). (a) Overview and (b) enlarged area. Cu-Fe sulfide nodule (bright) composed largely of bornite (Bn). Skeletal crystals are Fe-oxides, mainly wüstite (Wus, brighter grey) and some magnetite (darker grey). Matrix is prismatic fayalite (Fe-olivine, Fa).

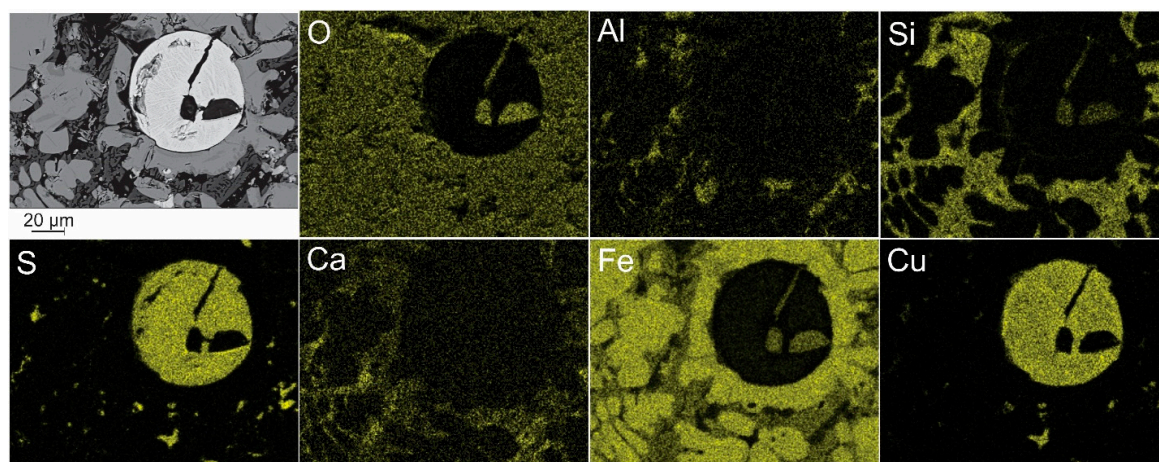


Figure 11. SEM-EDS maps of magnetic slag, of the area displayed in Figure 10b. First image is SEM-BSE.

A second magnetic sample (Figure 2b) was also dominantly composed of skeletal iron-oxides (bright phases in Figure 12a,b), in a matrix of prismatic fayalite (darker in Figure 12a,b). The SEM identification of phases was based on EDS spectra (Figure 13). The dark matrix, composed of Fe, Si and O is fayalite (Figure 13a). The bright nodules (Figure 12c,d, corresponding to the skeletal crystals in Figures 10a and 12a) have been identified as brighter wüstite with a high Fe-O ratio (Figure 13b) and darker magnetite with a lower Fe-O ratio (Figure 13c). Magnetite is concentrated on the periphery and along fractures of wüstite (Figure 12d). These minerals confirm the XRD analyses on bulk samples (Figure 3b). Occasionally, also in this sample, there were inclusions of bornite (very bright regions in Figure 12b,d).

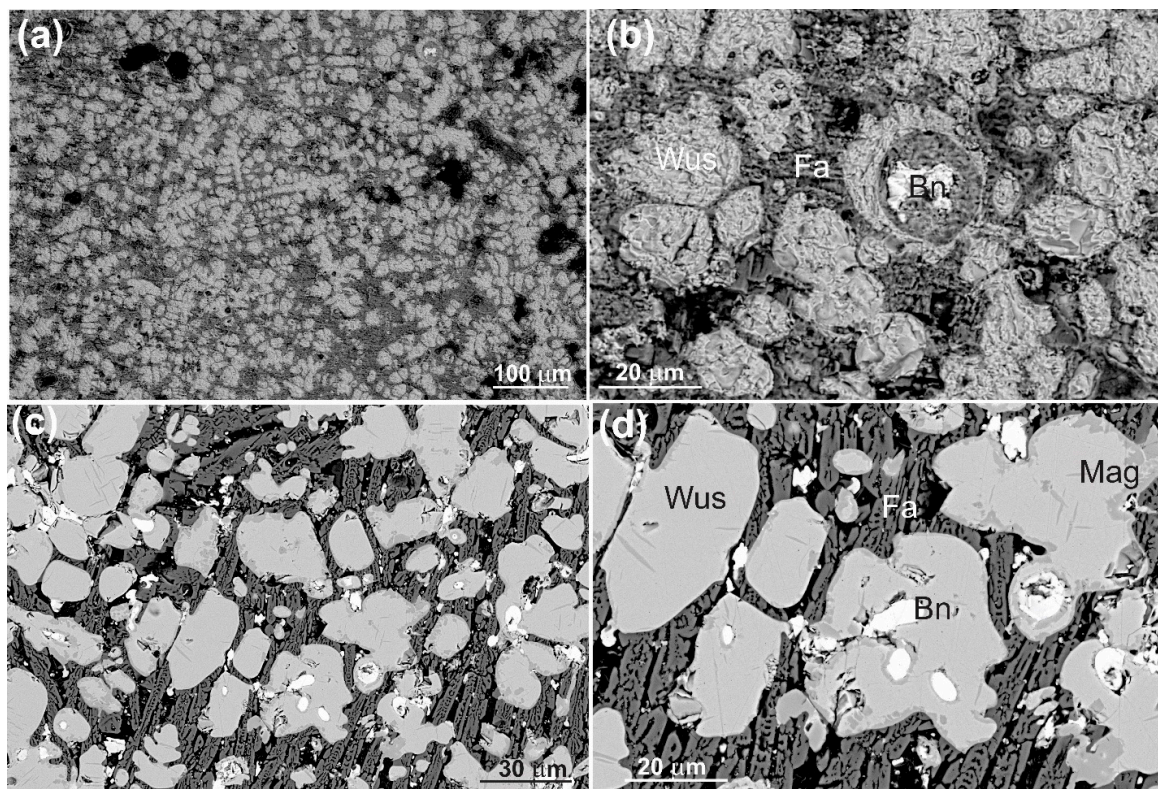


Figure 12. SEM-BSE images of magnetic slag. (a) Aggregations of wüstite (bright) in a fayalite matrix (dark). (b) Enlarged view of a region with wüstite (Wus) and fayalite (Fa) and some bornite (Bn) surrounded by fayalite. (c) Region with rounded wüstite/magnetite crystals (grey) and a skeletal fayalite matrix (dark). (d) Enlarged area of (c) with wüstite (Wus, brighter), magnetite (Mag, darker), some crystals with local bornite (Bn, white). Black is porosity. Images (a,b) were taken at variable vacuum, no carbon coat; (c,d) at high vacuum with carbon coat.

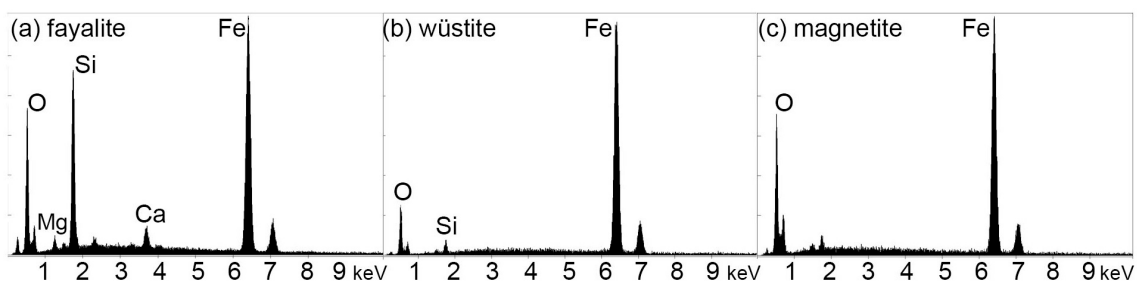


Figure 13. Selected SEM-EDS spectra from Figure 12d illustrating composition of magnetic Casaccia slag. (a) fayalite, (b) wüstite (high Fe/O ratio); (c) magnetite (lower Fe/O ratio). Only K α and L α peaks are labeled; vertical axis is count intensity.

To ascertain the phase identification of crystals at the micrometer scale microbeam synchrotron X-ray diffraction was used on two samples (Figure 2b,e). The beamsize was comparable to the particle sizes and diffractions occurred as fairly sharp spots on Debye rings, rather than continuous rings (left side of Figure 14), except for fine-grained copper (Figure 14b) and goethite (Figure 14c). On the right side of Figure 14 identified phases are highlighted with color circles. Bornite and pyrrhotite were confirmed in regions with metal-rich clusters of the non-magnetic sample (Figure 14a). Bornite and fine-grained elemental copper (fcc) occurred locally (Figure 14b). In the magnetic sample wüstite, magnetite and fayalite could be documented (Figure 14c). In addition there is a minor fraction of fine-grained goethite, probably formed as alteration of iron oxides.

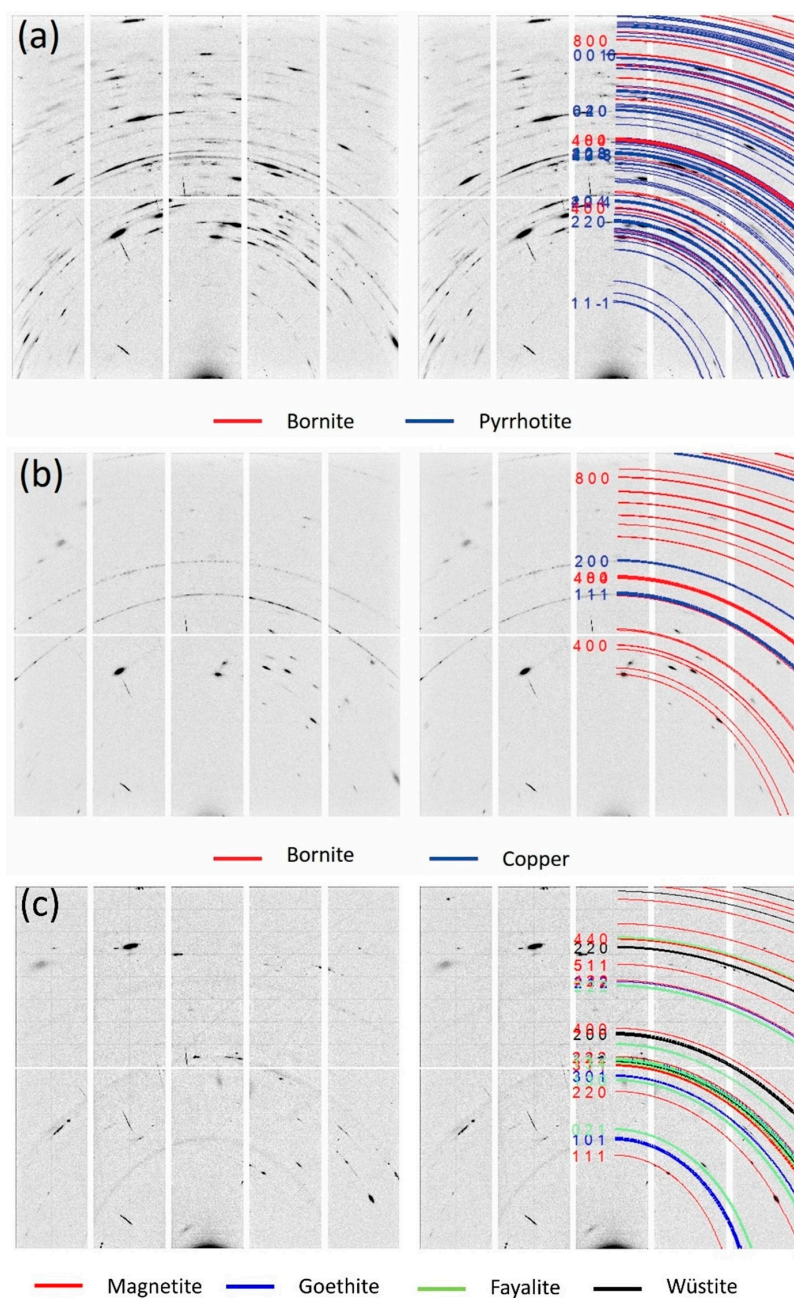


Figure 14. Microfocus synchrotron X-ray diffraction images of (a,b) non-magnetic and (c) magnetic slag. On the left side is the diffraction image, on the right side mineral phases are superposed and identified with colors; (a) corresponds to the circular region in Figure 8b, (b) to left side of Figure 8d and (c) to Figure 12d.

4. Discussion

4.1. Geochemistry of Copper Slags

Copper ores were processed most likely in small bloomery furnaces [36–40] at temperatures 1200–1400 °C [41]. Charcoal used in the furnaces was produced locally in heaps by pyrolysis of fir wood.

The geochemistry of copper slags has been explored in detail, both experimentally and based on thermodynamics [42,43]. Figure 15 displays a Fe-Cu-S phase diagram [43–45] with pyrrhotite and bornite coexisting at 700 °C. At higher temperature melting occurs [45]. The temperature of the Mg-rich core of olivine crystallizing from a melt is about 1200 °C [46]. The prismatic euhedral morphologies of olivine transforming to an acicular/dendritic pattern (Figures 4a and 8a) suggest initially relatively slow cooling rates at equilibrium conditions changing to a higher degree of undercooling as documented experimentally and with models for olivine crystallizing from melt [47–50]. Such microstructures were also described in modern copper slags [51].

The log f_{O_2} -temperature phase diagram (Figure 16) illustrates a likely fugacity of -15 at temperatures of ~ 1000 °C for the magnetic slag [52,53] to account for the prevalence of wüstite relative to magnetite. Some goethite documented with X-ray microdiffraction (Figure 14c) may be due to secondary oxidation.

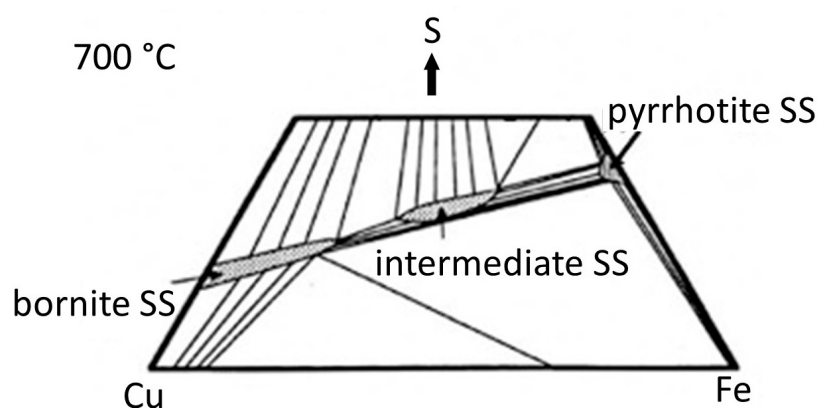


Figure 15. 700 °C isothermal section of Fe-Cu-S phase diagram. SS solid solution, based on Yund and Kullerud [44].

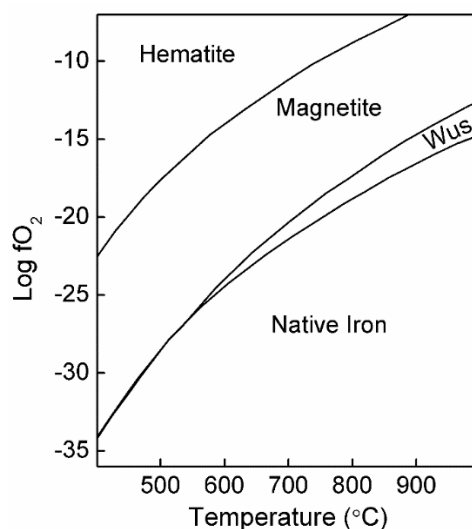


Figure 16. Log f_{O_2} -temperature phase diagram for Fe-O; Wus is wüstite. Modified from Miyashiro [52].

4.2. Ore Deposits

Metal ore deposits in Graubünden (E-Switzerland) have been explored by Schmidt [54] and then in more detail by Escher [28], Grünenfelder [29] and Dietrich [30]. These studies focus on mining activities in the 19th century, most of which were soon abandoned because they were not profitable. The main copper ore is chalcopyrite. Minor bornite has been described in the Suretta nappe at Alp Ursera near Andeer [28], at Piz Grisch [29] and the East-Alpine Silvretta nappe at Sertig and Lavin [28].

More closely related to Casaccia are historic and prehistoric Cu-Fe mines in the Oberhalbstein, associated with ophiolites and serpentinites of the Pennine Platta nappe such as Colm da Bovs (Tinzen), Marmorera, Crap Fess and Alp Tgavretga S of Bivio [30]. Close to the Mota Farun locality in Val Bregaglia, chalcopyrite has been described in prasinites near Piz Lizun [55] and Val Perossa [56]. The most likely source of the copper ore is chalcopyrite in metasedimentary layers of the Lizun nappe, the southern Platta nappe, probably associated with serpentinites, where pentlandite (Ni-S) has been identified [30].

We have a closer look at two localities. First an ore deposit in the vicinity of Alp Tgavretga near Septimer Pass (Swiss coordinates 768.96/144.27) at the contact of greenschists with serpentinites in the Platta nappe (samples Brg1828, 1829). This ore was exploited more recently, in the 19th century, but without much success [27]. Figure 17a shows a red layer very rich in sulfides and with a very high density. In hand specimens chalcopyrite (Figure 17b) and a malachite/azurite alteration (Figure 17c) can be observed. SEM-BSE images document abundant chalcopyrite (Figure 18a,c) with transformation to magnetite, and in a matrix of chlorite. Locally chromium spinel has been identified (Figure 18b). Other ore minerals are pyrite, pyrrhotite and ilvaite [30]. It is conceivable that material from Alp Tgavretga was transported across the Septimer Pass, southwards, because the forests above Casaccia are the closest providers of fuel for processing.

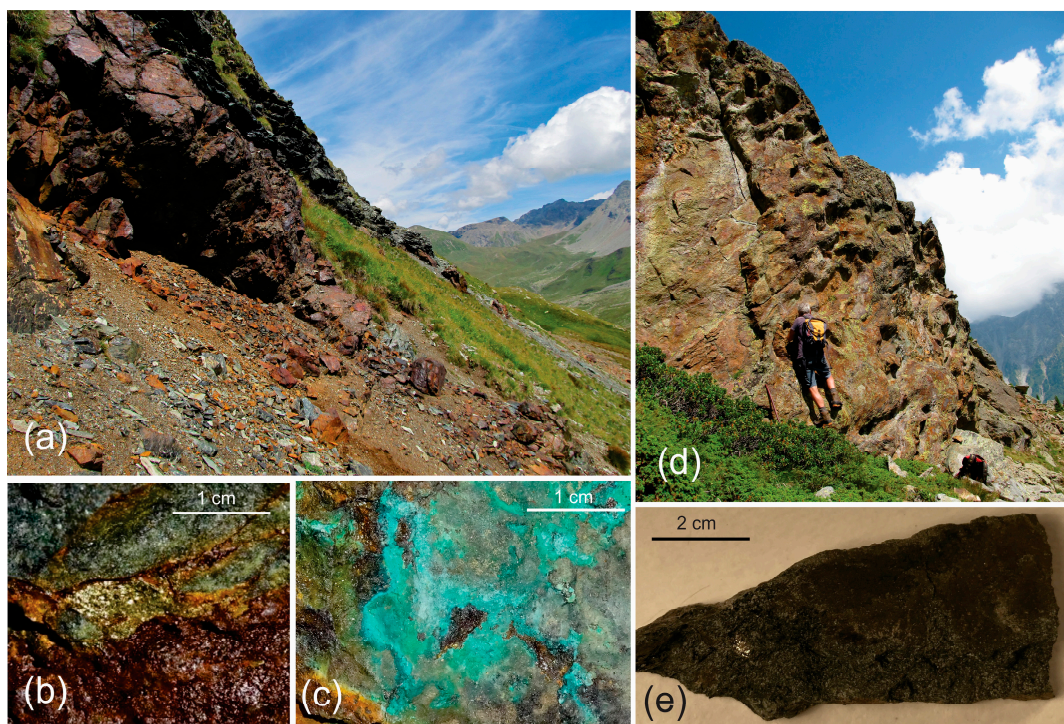


Figure 17. Images of ore deposits. (a–c) Alp Tavretga; (a) outcrop with red ore concentration; (b) hand specimen with chalcopyrite and magnetite; (c) copper ore altered to malachite. (d,e) Val Perossa; (d) outcrop with ore-rich layers; (e) hand specimen with pyrite in schist.

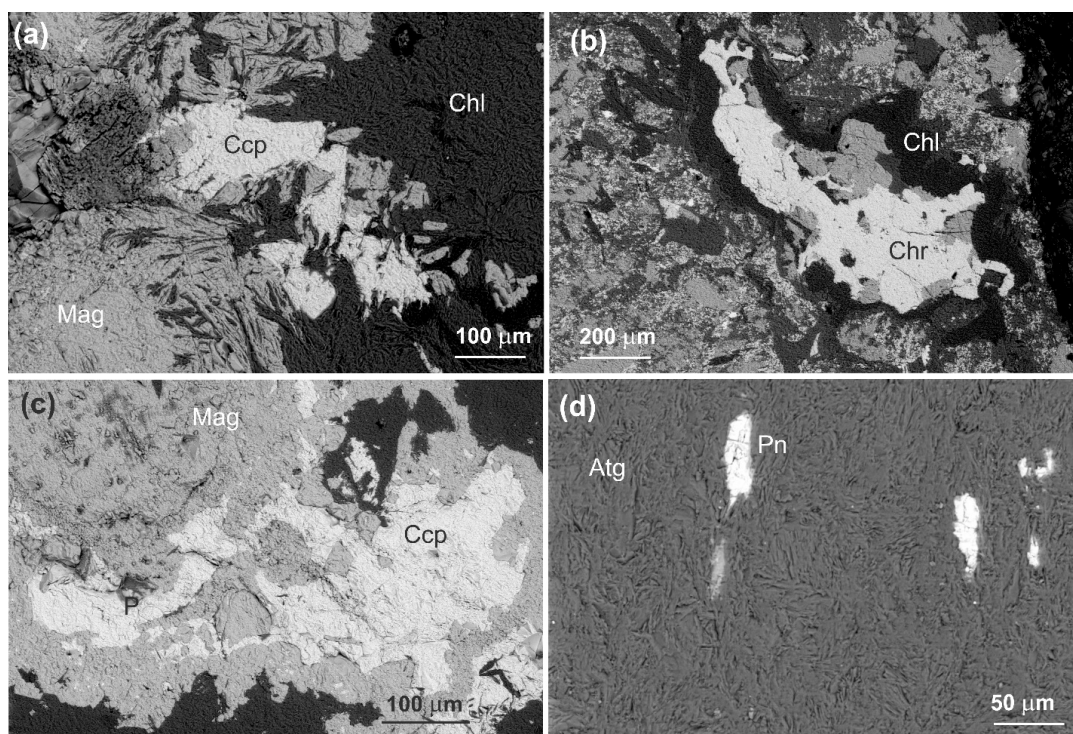


Figure 18. Microstructures in ore sample Brg1828 from Alp Tgavretga (a–c). SEM-BSE images. (a) chalcopyrite (Ccp, bright), magnetite (Mag, grey) and chlorite (Chl, dark). (b) Chromite (Chr) surrounded by chlorite (Chl). (c) chalcopyrite (Ccp, bright) and pyrite (P) transforming to magnetite (Mag, grey). (d) Serpentinite Brg1800 from Blaunca/Plaun dal Sel with pentlandite (Pn) in a matrix of antigorite (Atg).

Another locality is Val Perossa (formerly Val Parossa, Swiss coordinates 769.5/138.5, samples Brg1821, 1822), which contains a red zone of ore-rich greenschists (hence the name “rossa”) that was explored for ore around 1600 under the direction of the Vertemate family in Piuro [24,56] (Figure 17d). Most of the ore is pyrite (Figure 17e) but SEM observations document local concentrations of chalcopyrite associated with pyrite (Figure 19). Here the sulfides also oxidized, producing red iron hydroxides (goethite-lepidocrosite) responsible for the red color. Locally sphalerite (ZnS) was observed (Figure 19b). The matrix is composed of chlorite, muscovite, clinozoisite, albite, with inclusions of apatite and titanite. The same zone could continue towards Casaccia but may be covered by moraines, Quaternary debris, soils and forests.

Small amounts of pentlandite were observed in the Mota Farun slags (e.g., Figures 4f and 8d). Nickel is mainly observed in ultramafic rocks such as serpentinites in the western Alps [57] and serpentinitized ultramafics in Western Australia [58]. In a serpentinite from the Platta nappe at Blaunca near Grevasalvas, pentlandite has been documented (Figure 18d) and it is likely that minerals from serpentinites were added to ore processing, with slag compositions rich in magnesium and iron. This does not imply that pentlandite was significant for the ore production.

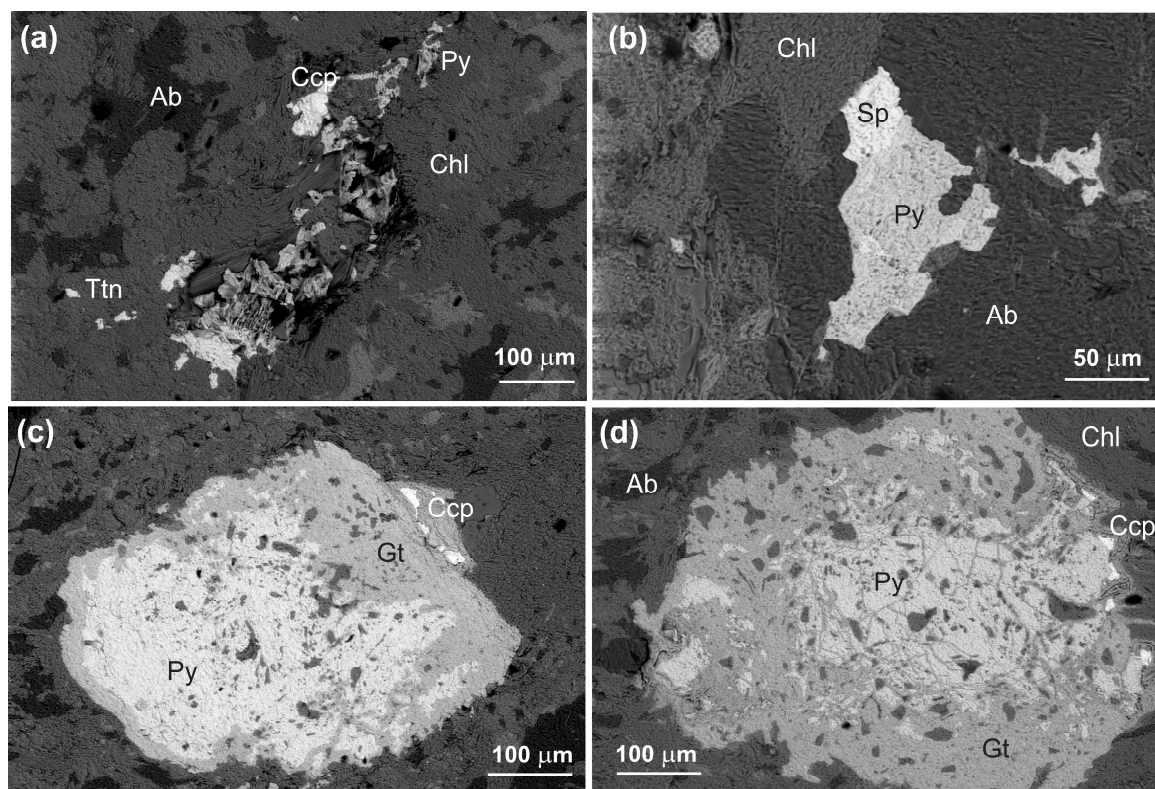


Figure 19. Microstructures in ore samples from Val Perossa (Brg1822). SEM-BSE images. (a) Pyrite (Py, grey), chalcopyrite (Ccp), titanite (bright spots on lower left, Ttn) and albite (Ab, black) in a matrix of chlorite (Chl); (b) Pyrite (Py) with sphalerite (Sp). (c,d) Pyrite (Py) altered to goethite (Gt) with regions of chalcopyrite (Ccp, bright spots on right side).

4.3. Prehistoric Copper Mining in the Eastern Alps

Significant prehistoric copper mining occurred in the Oberhalbstein, north of the Casaccia locality [12,26,59–61], in the Inn valley and Silvretta region [14–16,18,62], and around Luserna in Trentino-Italy [19–21]. The Bronze Ages are based on radiocarbon dating of wood inclusions in slags and go back to ~3000–2000 BC [22]. The microstructures and composition of slags from Luserna [20] show many similarities with the two Casaccia copper slags described here. It is likely that they are also Prehistoric, though no age determinations have been performed and there is no proof of that assumption. Contrary to the Oberhalbstein or Luserna the copper production at Casaccia was also on a much smaller scale. The bulk chemical composition of the Casaccia slags, rich in Fe, Si, with significant Mg, but poor in Ca and alkalis corresponds to other Alpine slags resulting from copper production [22]. The main phases in the two Casaccia slags are olivine-fayalite, wüstite, pyrrhotite, bornite, magnetite and copper. No quartz or feldspars were identified, which are major phases in the surrounding rocks of the Lizun nappe.

4.4. A Discussion of Analytical Methods

Scanning electron microscopy, particularly with backscatter imaging revealed complex microstructures in these Alpine slags. With EDS spectra it was possible to identify crystallites which are often at the submicron scale. Particularly important has been synchrotron microfocus synchrotron X-ray diffraction for unambiguous identifications of crystallites in extremely fine-grained materials. Similar methods have been applied to characterize other archeological materials such as Roman concrete [63] and Anthropocene products such as debris from nuclear explosions [64].

5. Conclusions

The Mota Farun slags are the first evidence for copper production in the Bergell Alps. In this study we explore compositions and microstructures of phases with modern methods used in materials science and mineralogy. Microstructures observed with scanning electron microscopy reveal complex conditions of formation such as olivine transforming from a euhedral to a dendritic morphology and intergrowth of pyrrhotite and bornite in globules. Magnetic slags display intricate intergrowths of wüstite and magnetite in a matrix largely composed of fayalite. Interestingly several slag samples from the same locality display very similar microstructures. The investigation may inspire others to apply similar methods to characterize different types of ancient slags to establish a data base to explore variations due to different ore compositions and production details.

Author Contributions: H.-R.W. initiated this study and prepared a draft of the manuscript. R.Y. was involved in all experiments and data analysis. N.T. conducted synchrotron experiments at the Advanced Light Source. D.B. and W.H. made critical contributions to sample collection.

Funding: H.-R.W. is appreciative for support from the National Science Foundation (EAR 1343908) and the Department of Energy (DE-FG02-05ER15637). R.Y. acknowledges support from the Industrial Key Scientific and Technological Project, Shaanxi, China (No. 2015GY101).

Acknowledgments: We acknowledged access to beamline 12.3.2 of the Advanced Light Source, which is a DOE Office of Science User Facility under contract no. DE-AC02-05CH11231, and the Zeiss EVO SEM at the Department of Earth and Planetary Science, UC Berkeley. Tim Teague helped with sample preparation as well as SEM and XRD analyses. We are thankful to the editor and two reviewers whose comments helped us improve the manuscript. We dedicate this paper to the memory of Remo Maurizio (1934–2017) who described this slag deposit and inspired this study. He contributed greatly to the natural history of the Bergell region throughout his career, including studies on minerals, plants and animals.

Conflicts of Interest: The authors declare no conflict of interest.

References

1. Artioli, G. *Scientific Methods and Cultural Heritage: An Introduction to the Application of Materials Science to Archaeometry and Conservation Science*; Oxford University Press: Oxford, UK, 2010; ISBN 978-0-19-172330-8.
2. Chiarantini, L.; Benvenuti, M.; Costagliola, P.; Fedi, M.E.; Guideri, S.; Romualdi, A. Copper production at Baratti (Populonia, southern Tuscany) in the early Etruscan period (9th–8th centuries BC). *J. Archaeol. Sci.* **2009**, *36*, 1626–1636. [[CrossRef](#)]
3. Craddock, P. Copper production in the Bronze Age of the British Isles. *Bull. Met. Mus.* **1992**, *18*, 3–28.
4. Erb-Satullo, N.L.; Gilmour, B.J.J.; Khakhtaiashvili, N. Late Bronze and Early Iron Age copper smelting technologies in the South Caucasus: The view from Ancient Colchis C. 1500–600 BC. *J. Archaeol. Sci.* **2014**, *49*, 147–159. [[CrossRef](#)]
5. Georgakopoulou, M.; Bassiakos, Y.; Philaniotou, O. Seriphos surfaces: A study of copper slag heaps and copper sources in the context of Early Bronze Age Aegean metal production. *Archaeometry* **2011**, *53*, 123–145.
6. O'Brien, W. *Prehistoric Copper Mining in Europe: 5500-500 BC*; Oxford University Press: New York, NY, USA, 2014; ISBN 978-0-19-960565-1.
7. Paynter, S. Regional variations in bloomery smelting slag of the Iron Age and Romano-British periods. *Archaeometry* **2006**, *48*, 271–292. [[CrossRef](#)]
8. Philaniotou, O.; Bassiakos, Y.; Georgakopoulou, M. Early Bronze Age Copper Smelting on Seriphos. In *Metallurgy: Understanding How, Learning Why: Studies in Honor of James D. Muhly*; Betancourt, P.P., Ferrence, S.C., Eds.; Prehistory Monographs; INSTAP Academic Press: Philadelphia, PA, USA, 2011; pp. 157–164, ISBN 978-1-931534-57-4.
9. Tylecote, R.F. *Early History of Metallurgy in Europe*; Addison-Wesley Longman Ltd.: London, UK; New York, NY, USA, 1987; ISBN 978-0-582-49195-3.
10. Pernicka, E.; Begemann, F.; Schmitt-Strecker, S.; Todorova, K.; Kuleff, I. Prehistoric copper in Bulgaria: Its composition and provenance. *Eurasia Antiq.* **1997**, *3*, 41–180.
11. Perucchetti, L.; Bray, P.; Dolfini, A.; Pollard, A.M. Physical barriers, cultural connections: Prehistoric metallurgy across the Alpine region. *Eur. J. Archaeol.* **2015**, *18*, 599–632. [[CrossRef](#)]

12. Schear, A. Untersuchungen zum prähistorischen Bergbau im Oberhalbstein (Kanton Graubünden). *Jahrbuch der Schweizerischen Gesellschaft für Ur- und Frühgeschichte* **2003**, *86*, 7–54.
13. Krause, R. The prehistoric settlement of the inneralpine valley of Montafon in Vorarlberg (Austria). *Preist. Alp.* **2007**, *42*, 119–136.
14. Lutz, J.; Bechter, D. Zur Mineralogie und Geochemie der Erze von Bartholomäberg und Silbertal im Montafon. *Archäol. Österr. Spez.* **2011**, *4*, 164–165.
15. Reitmaier, T.; Lambers, K.; Walser, C.; Zingman, I.; Haas, J.N.; Dietre, B.; Reidl, D.; Hajdas, I.; Nicolussi, K.; Kathrein, Y.; et al. Alpine Archäologie in der Silvretta. *Archäol. Schweiz* **2013**, *36*, 4–15.
16. Pernicka, E.; Lutz, J.; Stöllner, T. Bronze Age copper produced at Mitterberg, Austria, and its distribution. *Archaeol. Austriaca* **2016**, *1*, 19–56. [[CrossRef](#)]
17. Höppner, B.; Bartelheim, M.; Huijsmans, M.; Krauss, R.; Martinek, K.-P.; Pernicka, E.; Schwab, R. Prehistoric copper production in the Inn Valley (Austria), and the earliest copper in Central Europe. *Archaeometry* **2005**, *47*, 293–315. [[CrossRef](#)]
18. Klemm, S. *Montanarchäologie in den Eisenerzer Alpen, Steiermark: Archäologische und Naturwissenschaftliche Untersuchungen Zum Prähistorischen Kupferbergbau in der Eisenerzer Ramsau*; Verlag der Österreichischen Akademie der Wissenschaften: Wien, Austria, 2003; ISBN 978-3-7001-3147-2.
19. Artioli, G.; Angelini, I.; Tecchiati, U.; Pedrotti, A. Eneolithic copper smelting slags in the Eastern Alps: Local patterns of metallurgical exploitation in the Copper Age. *J. Archaeol. Sci.* **2015**, *63*, 78–83. [[CrossRef](#)]
20. Addis, A.; Angelini, I.; Nimis, P.; Artioli, G. Late Bronze Age copper smelting slags from Luserna (Trentino, Italy): Interpretation of the metallurgical process. *Archaeometry* **2016**, *58*, 96–114. [[CrossRef](#)]
21. Cierny, J. *Prähistorische Kupferproduktion in den südlichen Alpen: Region Trentino Orientale*; Dt. Bergbau-Museum: Bochum, Germany, 2008; ISBN 978-3-937203-38-6.
22. Metten, B. Beitrag zur spätbronzezeitlichen Kupfermetallurgie im Trentino (Südalpen) im Vergleich mit anderen prähistorischen Kupferschlacken aus dem Alpenraum. *Met. Boch.* **2003**, *10*, 1–122.
23. Bourgarit, D.; Rostan, P.; Burger, E.; Carozza, L.; Mille, B.; Artioli, G. The beginning of copper mass production in the Western Alps: The Saint-Veran mining area reconsidered. *Hist. Metall.* **2008**, *42*, 1–11.
24. Maurizio, R. Indagini su Vecchie Cave e Miniere in Bregaglia. *Quad. Grigionital.* **1972**, *41*, 1–71.
25. Wenk, H.R. The structure of the Bergell Alps. *Eclogae Geol. Helv.* **1973**, *66*, 255–291.
26. Della Casa, P.; Naef, L.; Turck, R. Prehistoric copper pyrotechnology in the Swiss Alps: Approaches to site detection and chaîne opératoire. *Quat. Int.* **2016**, *402*, 26–34. [[CrossRef](#)]
27. Von Salis, C.U. Über den Bergbau in Bünden. *Neue Samml.* **1806**, *2*, 491–561.
28. Escher, E. Erzlagerstätten und Bergbau im Schams, in Mittelbünden und im Engadin. *Beitr. Zur Geol. Schweiz Geotech. Ser.* **1935**, *18*, 120.
29. Grünenfelder, M. Petrographie des Roffnakristallins in Mittelbünden und seine Eisenvererzung. *Beitr. Zur Geol. Schweiz Geotech. Ser.* **1956**, *35*, 60.
30. Dietrich, V. Die Sulfidischen Vererzungen in den Oberhalbsteiner Serpentiniten: Ein. Beitrag zur Kenntnis der alpinen Metamorphosen und des Gebirgsbaues im südlichen Graubünden. *Beitr. Z. Geol. Schweiz Geotech. Ser.* **1972**, *49*, 128.
31. Staub, R. *Geologische Karte des Avers (Piz Platta–Duan), 1:50 000*; Geologische Spezial-Karte der Schweiz Nr. 115; Schweizerische Geologische Kommission: Bern, Switzerland, 1926.
32. Handy, M.R.; Herwegh, M.; Kamber, B.S.; Tietz, R.; Villa, I.M. Geochronologic, petrologic and kinematic constraints on the evolution of the Err-Platta boundary, part of a fossil continent-ocean suture in the Alps (Eastern Switzerland). *Schweiz. Mineral. Petrogr. Mitteilungen* **1996**, *76*, 453–474.
33. Lutterotti, L.; Vasin, R.; Wenk, H.R. Rietveld texture analysis from synchrotron diffraction images. I. Calibration and basic analysis. *Powder Diffr.* **2014**, *29*, 76–84. [[CrossRef](#)]
34. Tamura, N. Xmas: A versatile tool for analyzing synchrotron X-ray microdiffraction data. In *Strain and Dislocation Gradients from Diffraction*; London Imperial College Press: London, UK, 2013; pp. 125–155, ISBN 978-1-908979-62-9.
35. Kretz, R. Symbols for rock-forming minerals. *Am. Mineral.* **1983**, *68*, 277–279.
36. Elliott, J.F. Phase relationships in the pyrometallurgy of copper. *Metall. Mater. Trans. B* **1976**, *7*, 17–33. [[CrossRef](#)]

37. Fernández-Caliani, J.C.; Ríos, G.; Martínez, J.; Jiménez, F. Occurrence and speciation of copper in slags obtained during the pyrometallurgical processing of chalcopyrite concentrates at the Huelva Smelter (Spain). *J. Min. Metall. Sect. B Metall.* **2012**, *48*, 161–171. [[CrossRef](#)]
38. Karbowniczek, M.; Weker, W.; Suliga, I. Experimental metallurgical process in a slag pit bloomery furnace. *EuroREA* **2006**, *6*, 45–49.
39. Manasse, A.; Mellini, M.; Viti, C. The copper slags of the Capattoli Valley, Campiglia Marittima, Italy. *Eur. J. Mineral.* **2001**, *13*, 949–960. [[CrossRef](#)]
40. Tylecote, R.-F.; Austen, J.N.; Wrath, A.E. The mechanism of the bloomery process in shaft furnace. *J. Iron Steel Inst.* **1971**, *209*, 342–363.
41. Bachmann, H.G. *Early Copper Smelting Techniques in Sinai and in the Negev and Deduced Slag Investigations, in Scientific Studies in Early Mining and Extractive Metallurgy*; Craddock, P.T., Ed.; British Museum: London, UK, 1980.
42. Bachmann, H.-G. *The Identification of Slags from Archaeological Sites*; Occasional publication/Institute of Archaeology; Institute of Archaeology: London, UK, 1982; ISBN 978-0-905853-10-9.
43. Shishin, D.; Jak, E.; Deckerov, S.A. Thermodynamic assessment and database for the Cu-Fe-O-S system. *CALPHAD* **2015**, *50*, 144–160. [[CrossRef](#)]
44. Tsujimura, T.; Kitakaze, A. New phase relations in the Cu-Fe-S system at 800 °C; Constraint of fractional crystallization of a sulfide liquid. *Neues Jahrbuch für Mineralogie-Monatshefte* **2004**, *10*, 433–444. [[CrossRef](#)]
45. Yund, R.A.; Kullerud, G. Thermal stability of assemblages in the Cu-Fe-S system. *J. Petrol.* **1966**, *7*, 454–488. [[CrossRef](#)]
46. Bowen, N.L.; Schairer, J.F. The system MgO-FeO-SiO₂. *Am. J. Sci.* **1935**, *29*, 151–217. [[CrossRef](#)]
47. Donaldson, C.H. An experimental investigation of olivine morphology. *Contrib. Mineral. Petrol.* **1976**, *57*, 187–213. [[CrossRef](#)]
48. Faure, F.; Troiliard, G.; Nicollet, C.; Montel, J.-M. A developmental model of olivine morphology as a function of the cooling rate and the degree of undercooling. *Contrib. Mineral. Petrol.* **2003**, *145*, 251–263. [[CrossRef](#)]
49. Faure, F.; Schiano, P. Experimental investigation of equilibration conditions during forsterite growth and melt inclusion formation. *Earth Planet. Sci. Lett.* **2005**, *236*, 882–898. [[CrossRef](#)]
50. Faure, F.; Schiano, P.; Troiliard, G.; Nicollet, C.; Soulestin, B. Textural evolution of polyhedral olivine experiencing rapid cooling rates. *Contrib. Mineral. Petrol.* **2007**, *153*, 405–416. [[CrossRef](#)]
51. Mihailova, I.; Mehandjiev, D. Characterization of fayalite from copper slags. *J. Univ. Chem. Technol. Metall.* **2010**, *45*, 317–326.
52. Miyashiro, A. Oxidation and reduction in the Earth's crust with special reference to the role of graphite. *Geochim. Cosmochim. Acta* **1964**, *28*, 717–729. [[CrossRef](#)]
53. Khurshid, H.; Chandra, S.; Li, W.; Phan, M.H.; Hadjipanayis, G.C.; Mukherjee, P.; Srikanth, H. Synthesis and magnetic properties of core/shell FeO/Fe₃O₄ nano-octopods. *J. Appl. Phys.* **2013**, *113*, 17B508. [[CrossRef](#)]
54. Schmidt, C. *Texte Explicatif de la Carte des Gisements des Matières Premières Minérales de la Suisse: 1:500,000*; Commission geotechnique Suisse; Birkhäuser: Basel, Switzerland, 1920.
55. Maurizio, R.; Meisser, N. Neue Mineralien des Bergells (Schweiz-Italien). *Schweiz. Strahler* **1993**, *9/11*, 525–577.
56. Bedognè, F.; Maurizio, R.; Montrasio, A.; Sciesa, E. *I Minerali della Provincia di Sondrio e della Bregaglia Grigionesa: Val Bregaglia, Val Masino, Val Codera e Valle Spluga*; Bettini: Sondrio, Italy, 1995.
57. Malvoisin, B.; Chopin, C.; Baronnet, A.; Brunet, F.; Bezacier, L.; Guillot, S. Fe–Ni-rich silicate aggregates formed after sulfides in high-pressure serpentinites. *J. Petrol.* **2017**, *58*, 963–978. [[CrossRef](#)]
58. Nickel, E.H.; Thornber, M.R. Chemical constraints on the weathering of Serpentinites containing nickel-iron sulphides. *J. Geochem. Explor.* **1977**, *8*, 235–245. [[CrossRef](#)]
59. Reitmaier-Naef, L.; Rouven, T.; Casa, P.D. Prähistorische Kupfergewinnung im Oberhalbstein. *Minaria Helv.* **2015**, *36*, 35–54.
60. Turck, R.; Della Casa, P.; Naef, L. Prehistoric Copper Pyrotechnology in the South-Eastern Swiss Alps: An Overview on Previous and Current Research. In *De l'âge du Fer à l'usage du verre. Mélanges offerts à Gilbert Kaenel, dit "Auguste", à l'occasion de son 65e anniversaire*; Bullinger, J., Crotti, P., Huguenin, C., Eds.; Cahiers de l'Archéologie Romande 151: Lausanne, Switzerland, 2014; pp. 249–257, ISBN 978-2-88028-151-9.
61. Wyss, R. Die Höhensiedlung Motta Vallac im Oberhalbstein (Salouf Gr). *Schweiz. Ges. für Ur- Frühgeschichte* **1982**, *5*, 77–82.
62. Lutz, J.; Pernicka, E. Prehistoric copper from the Eastern Alps. *Open J. Archaeom.* **2013**, *1*, 122–127. [[CrossRef](#)]

63. Jackson, M.D.; Mulcahy, S.R.; Chen, H.; Li, Y.; Li, Q.; Cappelletti, P.; Wenk, H.-R. Phillipsite and Al-tobermorite mineral cements produced through low-temperature water-rock reactions in Roman marine concrete. *Am. Mineral.* **2017**, *102*, 1435–1450. [[CrossRef](#)]
64. Wannier, M.M.A.; de Urreiztieta, M.; Wenk, H.-R.; Stan, C.V.; Tamura, N.; Yue, B. Fallout melt debris and aerodynamically-shaped glasses in beach sands of Hiroshima Bay, Japan. *Anthropocene* **2019**, *25*, 100196. [[CrossRef](#)]



© 2019 by the authors. Licensee MDPI, Basel, Switzerland. This article is an open access article distributed under the terms and conditions of the Creative Commons Attribution (CC BY) license (<http://creativecommons.org/licenses/by/4.0/>).